

Improvement of valley splitting and valley injection efficiency for graphene/ferromagnet heterostructure

Longxiang Xu(徐龙翔), Wengang Lu(吕文刚), Chen Hu(胡晨), Qixun Guo(郭奇勋), Shuai Shang(尚帅), Xiulan Xu(徐秀兰), Guanghua Yu(于广华), Yu Yan(岩雨), Lihua Wang(王立华), Jiao Teng(滕蛟)

Citation: Chin. Phys. B . 2020, 29(7): 077304 . **doi:** 10.1088/1674-1056/ab8db2
Journal homepage: http://cpb.iphy.ac.cn; http://iopscience.iop.org/cpb

What follows is a list of articles you may be interested in

Comparative study on transport properties of N-, P-, and As-doped SiC nanowires: Calculated based on first principles

Ya-Lin Li(李亚林), Pei Gong(龚裴), Xiao-Yong Fang(房晓勇)

Chin. Phys. B . 2020, 29(3): 037304 . **doi:** 10.1088/1674-1056/ab6c4c

Tunneling magnetoresistance in ferromagnet/organic-ferromagnet/metal junctions

Yan-Qi Li(李彦琪), Hong-Jun Kan(阚洪君), Yuan-Yuan Miao(苗圆圆), Lei Yang(杨磊), Shuai Qiu(邱帅), Guang-Ping Zhang(张广平), Jun-Feng Ren(任俊峰), Chuan-Kui Wang(王传奎), Gui-Chao Hu(胡贵超)

Chin. Phys. B . 2020, 29(1): 017303 . **doi:** 10.1088/1674-1056/ab5d02

Effects of oxygen vacancy concentration and temperature on memristive behavior of $SrRuO_3$/Nb:$SrTiO_3$ junctions

Zhi-Cheng Wang(王志成), Zhang-Zhang Cui(崔璋璋), Hui Xu(徐珲), Xiao-Fang Zhai(翟晓芳), Ya-Lin Lu(陆亚林)

Chin. Phys. B . 2019, 28(8): 087303 . **doi:** 10.1088/1674-1056/28/8/087303

Phase diagram characterized by transmission in a triangular quantum dot

Jin Huang(黄金), Wei-Zhong Wang(王为忠)

Chin. Phys. B . 2018, 27(11): 117303 . **doi:** 10.1088/1674-1056/27/11/117303

Transport spectroscopy through dopant atom array in silicon junctionless nanowire transistors

Xiao-Song Zhao(赵晓松), Wei-Hua Han(韩伟华), Yang-Yan Guo(郭仰岩), Ya-Mei Dou(窦亚梅), Fu-Hua Yang(杨富华)

Chin. Phys. B . 2018, 27(9): 097310 . **doi:** 10.1088/1674-1056/27/9/097310

RAPID COMMUNICATION

Improvement of valley splitting and valley injection efficiency for graphene/ferromagnet heterostructure*

Longxiang Xu(徐龙翔)[1], Wengang Lu(吕文刚)[2,3,†], Chen Hu(胡晨)[4], Qixun Guo(郭奇勋)[1], Shuai Shang(尚帅)[1], Xiulan Xu(徐秀兰)[1], Guanghua Yu(于广华)[1], Yu Yan(岩雨)[5], Lihua Wang(王立华)[6], and Jiao Teng(滕蛟)[1,‡]

[1] *Department of Materials Physics and Chemistry, University of Science and Technology Beijing, Beijing,* 100083, *China*
[2] *Institute of Physics, Chinese Academy of Sciences, Beijing* 100190, *China*
[3] *Beijing Key Laboratory for Nanomaterials and Nanodevices, Beijing* 100190, *China*
[4] *Center for the Physics of Materials and Department of Physics, McGill University, Montreal, Quebec H3A* 2T8, *Canada*
[5] *Corrosion and Protection Center, Key Laboratory for Environmental Fracture (MOE), University of Science and Technology Beijing, Beijing* 100083, *China*
[6] *Institute of Microstructure and Property of Advanced Materials, Beijing Key Laboratory of Microstructure and Property of Advanced Materials, Beijing University of Technology, Beijing* 100124, *China*

(Received 11 April 2020; revised manuscript received 22 April 2020; accepted manuscript online 28 April 2020)

The valley splitting has been realized in the graphene/Ni heterostructure with the splitting value of 14 meV, and the obtained valley injecting efficiency from the heterostructure into graphene was 6.18% [*Phys. Rev. B* **92** 115404 (2015)]. In this paper, we report a way to improve the valley splitting and the valley injecting efficiency of the graphene/Ni heterostructure. By intercalating an Au monolayer between the graphene and the Ni, the split can be increased up to 50 meV. However, the valley injecting efficiency is not improved because the splitted valley area of graphene moves away from the Fermi level. Then, we mend the deviation by covering a monolayer of Cu on the graphene. As a result, the valley injecting efficiency of the Cu/graphene/Au/Ni heterostructure reaches 10%, which is more than 60% improvement compared to the simple graphene/Ni heterostructure. Then we theoretically design a valley-injection device based on the Cu/graphene/Au/Ni heterostructure and demonstrate that the valley injection can be easily switched solely by changing the magnetization direction of Ni, which can be used to generate and control the valley-polarized current.

Keywords: valleytronics, two-dimensional materials, valley-polarized transport

PACS: 73.63.–b, 72.80.Vp, 85.75.–d **DOI:** 10.1088/1674-1056/ab8db2

1. Introduction

Honeycomb Dirac materials have twofold-degenerate band structures with inequivalent K and K' valleys, which are located respectively at the corners of the hexagonal Brillouin zone (BZ).[1–5] Valley scattering between the K and K' is suppressed due to the large separation between the two valleys. It is fairly stable for electrons sitting in a certain valley. We believe that this feature of valley would provide a firm foundation for manipulation of the valley degree of freedom and may pave a way for the application of valleytronics in the future.

Analogous to the charge degree of freedom in the traditional microelectronics and the spin degree of freedom in spintronics, the valley degree of freedom can also transmit information, therefore, it triggers a new subject of valleytronics and paves a new way for the future information technology.[6–12] The premise of valleytronics is getting polarized valleys. However, the K and K' valleys are normally degenerate. So lifting the degenerated K and K' valleys is crucial.

Many ways have been proposed to lift the degenerated valleys till now. Strong magnetic fields were reported to be able to generate valley splits.[9–12] However, the required giant magnetic fields and tiny splits (0.1–0.2 meV/T) limit the application. Another way is the circularly polarized light method, which excites specific valleys.[13–19] Among the honeycomb Dirac material family, graphene is a particular member and often takes the role to represent the family, due to its simple structure, unique physical properties, and the greatest potential in future applications. However, the circularly polarized light method can not be applied to graphene based systems, because it demands a particular gap that graphene does not have.

For practical application, we have proposed a general idea to obtain polarized valleys in graphene and realize valley injection into graphene through an example of the Ni/graphene

*Project supported by the National Key R&D Program of China (Grant No. 2017YFF0206104), the National Natural Science Foundation of China (Grant No. 51871018), Beijing Laboratory of Metallic Materials and Processing for Modern Transportation, the Opening Project of Key Laboratory of Microelectronics Devices & Integrated Technology, Institute of Microelectronics of Chinese Academy of Sciences, Beijing Natural Science Foundation, China (Grant No. Z180014), and Beijing Outstanding Young Scientists Projects, China (Grant No. BJJWZYJH01201910005018). We gratefully acknowledge the Chinese Academy of Sciences for providing computation facilities.

†Corresponding author. E-mail: wglu@iphy.ac.cn
‡Corresponding author. E-mail: tengjiao@mater.ustb.edu.cn

© 2020 Chinese Physical Society and IOP Publishing Ltd

heterostructure in our previous work.[6] However, the linear dispersion of the π states of graphene is destroyed to a certain extent by the strong interaction between the graphene and Ni,[20] which limits the injection efficiency. In this paper, we will improve our former Ni/graphene heterostructure by intercalating a monolayer Au to preserve the unique structure of the graphene, and by covering a Cu layer to fix the Dirac point around the Fermi level. Finally, we propose a new valley injector based on the Cu/graphene/Au/Ni heterojunction.

2. Methods

The electronic structures and transport properties are calculated by the software package NANODCAL, which combines the density functional theory and the non-equilibrium Green function.[21,22] We use the local density approximation[23] for the exchange correlation and the double-zeta polarized atomic orbits as the basis sets for all the atom species in all calculations. The cut-off energy for the real space grid is taken as 3000 eV and a k-point mesh of $24\times14\times1$ along the X, Y, and Z directions is used for the k-sampling. The external magnetic fields are responded by the spin directions of the nickel atoms. The spin polarizations of the bulk Ni are calculated self-consistently. Convergences are considered to be achieved when the total energy, Hamiltonian matrix, and density matrix all reach the precision of 10^{-5} arb. units.

3. Results and discussion

We start the discussion from the graphene/Au/Ni heterostructure as shown in Fig. 1(a). There are two possible configurations for the Au monolayer. The first one is reported in an early Au intercalation work, where the Au atoms form a two-dimensional hexagonal layer in commensuration with the Ni (111) substrate.[20] In this configuration, the Au–Au bond length is 2.84 Å, which matches well with the experimental value of 2.87 Å. However, the three Au atoms in a unit cell stand respectively on the A-, B-, and H-sites of the graphene, which preserves the A–B symmetry of the graphene, making the valley resolved property disappear.

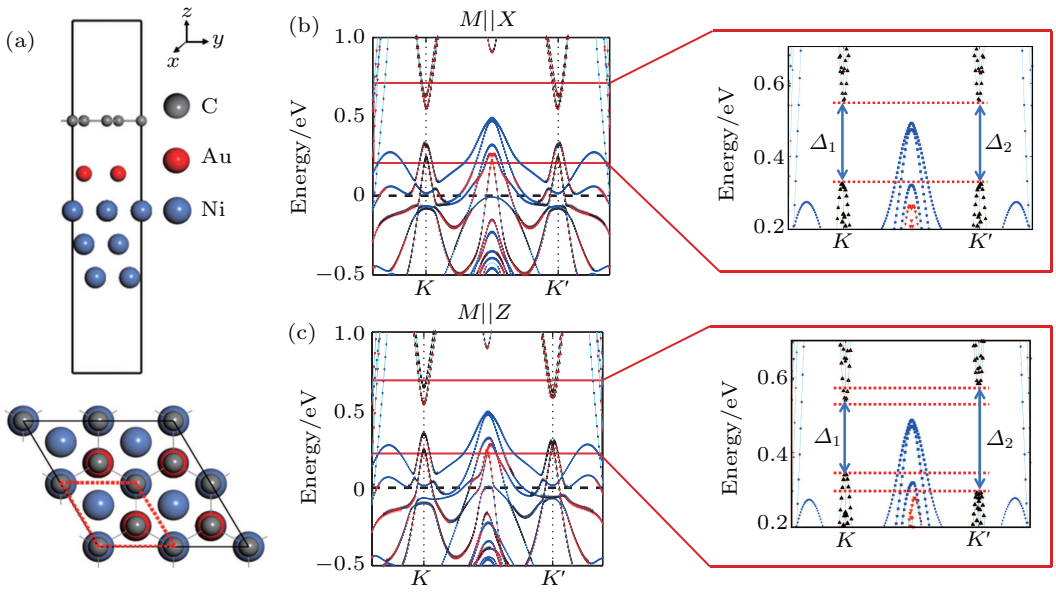


Fig. 1. Atomic geometry and band structures of the graphene/Au/Ni (111) heterostructure. (a) Side and top views of the atomic structure of the graphene/Au/Ni (111) heterostructure. The gray, red, and blue balls respectively denote the C, Au, and Ni atoms. All of the Au atoms are on the top sites of a specific sub-lattice. Valley-resolved band structures of the graphene/Au/Ni heterostructure for $M\,\|\,X$ (b) and $M\,\|\,Z$ (c). The black, blue, and red dotted lines represent the orbital contributions of the p orbits of the C atoms, the 3d orbits of the Ni atoms, and 5d orbits of Au, respectively. The red rectangles in (b) and (c) are replotted in the right to show the valley splitting.

In the other possible configuration, on one side of the Au monolayer, the Au atoms form a two-dimensional epitaxial layer from the Ni (111) substrate, and on the other side, stand on a certain sub-lattice of graphene, which completely breaks the A–B symmetry, as shown in Fig. 1(a). So we consider only this configuration. The lattice constants of the graphene and the Ni (111) surface are set to be 2.46 Å, which is close to the experiment values and makes the interface almost have no mismatch. The distances between the Au layer and the graphene layer, the Ni layer and the Au layer are taken as 2.5 Å and 2.32 Å, respectively. Figures 1(b) and 1(c) plot the valley-resolved band structure of the graphene/Au/Ni heterostructure. For clarity, the Fermi energy $E_{\rm F}$ is shifted to zero and the momentum is along the G–K–K'–G direction in all of the band plots in this paper. Strong spin–orbital coupling transfers from the Au 5d orbits to the carbon 2p orbits because of the hybridization between them. As a result, the spin–orbit splitting becomes as large as 100 meV, which coincides with the experiments,[24–26] and the valley splitting is enhanced and the maximum reaches about 50 meV, which is three times

larger than that of the Ni/graphene system without the Au intercalation. Due to the screening effect of the Au atoms, the linear dispersion of the graphene is partially recovered. But the gaps, denote by Δ_1 and Δ_2 respectively, hold on at the K and K' valleys, because of the A–B lattice symmetry breaking. When $M \parallel X$ (in the graphene plane), $\Delta_1 = \Delta_2 = 200$ meV, and the two valleys at the K and K' points are degenerate, as shown in Fig. 1(b). However, when $M \parallel Z$ (perpendicular to the plane), the valley-splitting occurs with $\Delta_1 = 200$ meV and $\Delta_2 = 300$ meV, as shown in Fig. 1(c). This is because the valley magnetic moment only couples to the magnetic field or the magnetic moment in the perpendicular direction.[6]

Next, we consider the effect of Au concentration on the valley splitting, since the shapes and positions of the graphene π bands are sensitive to the amount of intercalated Au atoms. At the high coverage of 1 monolayer (ML) (1 ML refers to 1 Au per Ni on the Ni (111) surface), the shapes of the Dirac cones are largely preserved. However, the conical points (defined as the midpoints of the gaps of the graphene π bands in this paper, the same as the definition in Ref. [20]) shift upward by 500 meV, indicating a large charge transfer from the graphene to the substrate, which is detrimental to the valley polarized transport because only the states near the Fermi level contribute to the current. With the reduction of the coverage of the Au atoms from 1 ML to 0.25 ML, the Dirac points gradually shift downward.[20] But without enough Au atoms to block the hybridization between the graphene and the Ni (111) substrate, the linearity of the graphene π bands is disrupted and the valley splitting disappears at low Au coverages.

From the above discussion, we know that the Au monolayer can keep the shape of the graphene bands and increase the valley splitting. But the Dirac points are about 500 meV higher than the Fermi level. To move the Dirac point down to the Fermi surface, we try to deposit a layer of Cu atoms upon the graphene, because electrons transfer from Cu to graphene at the graphene/Cu contact.[27] The distance between the Cu layer and the graphene layer is taken as 2.5 Å. When the Cu and Au atoms stand on the same sub-lattice of the graphene (A–A stacking), the valley splitting is only slightly smaller than that when the Cu and Au atoms on the opposite sublattices of the graphene (A–B stacking). So we only consider the A–B stacking case. As the black dashed lines show, in Figs. 2(a) and 2(b), the Dirac points shift to the vicinity of the Fermi level. Same as the above discussion, when we turn the magnetization direction of Ni from X to Z, the band structure changes from the valley degenerate state to the valley splitting state. The maximal valley splitting slightly reduces to 40 meV. In this Cu/graphene/Au/Ni structure, the shapes of the graphene π bands are largely preserved and the valley splitting occurs near the Fermi level, which makes it an ideal valley injector to realize valley polarized current.

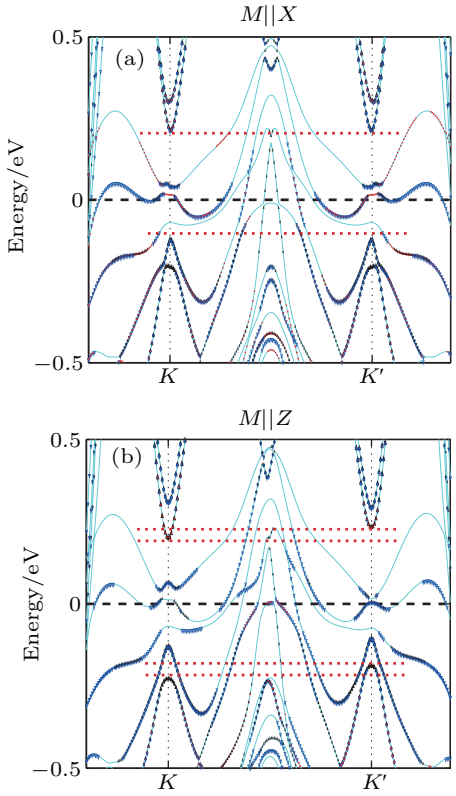


Fig. 2. Band structures of the Cu/graphene/Au/Ni heterostructure. (a) When $M \parallel X$, the two valleys are degenerate. (b) When $M \parallel Z$, the two valleys split.

To study the valley-related transport properties of the Cu/graphene/Au/Ni heterojunction, we design a system shown in Fig. 3(a). The left lead is the Cu/graphene/Au/Ni heterojunction as a valley injector, and the right lead is an individual graphene. The two leads extend to $-\infty$ and $+\infty$, respectively. The central scattering region including the heterojunction/graphene contact part has a length of 1.7 nm. The transport direction is along the armchair direction of the graphene (y direction). We compare the (E, k_x)-resolved transmission coefficients for $M \parallel X$ in Fig. 3(b) and $M \parallel Z$ in Fig. 3(d). In the two plots, the transmissions focus on $k_x = \pm 1/3$, which are exactly the valley positions. This is because the individual graphene in the right lead only has the states at K and K' near E_F, thus only the carriers at the same states in the left lead are allowed to transport to the right, leading to the sharp peaks at the valley positions. In addition, when $M \parallel X$, the transmissions in the two valleys are completely identical. However, when $M \parallel Z$, they are obviously different, which realizes the valley-polarized injection.

Additionally, the valley splittings as large as 40 meV occur around 200 meV and -200 meV, as shown in Fig. 3(c). Correspondingly, the transmission coefficients at the two valleys diverge exactly in the same energy regions. For example, in the red dotted-line-marked area in Fig. 3(d), located at $E = 0.2$–0.24 eV, the K valley has a larger transmission coefficient than the K' valley. The non-symmetric transmission between the two valleys can be explained by the band struc-

ture of the left lead, as shown in Fig. 3(c), where in the energy range of 0.2–0.24 eV, carriers in the K valley have extra conducting modes, marked by the red dotted line, then contribute the extra transmission.

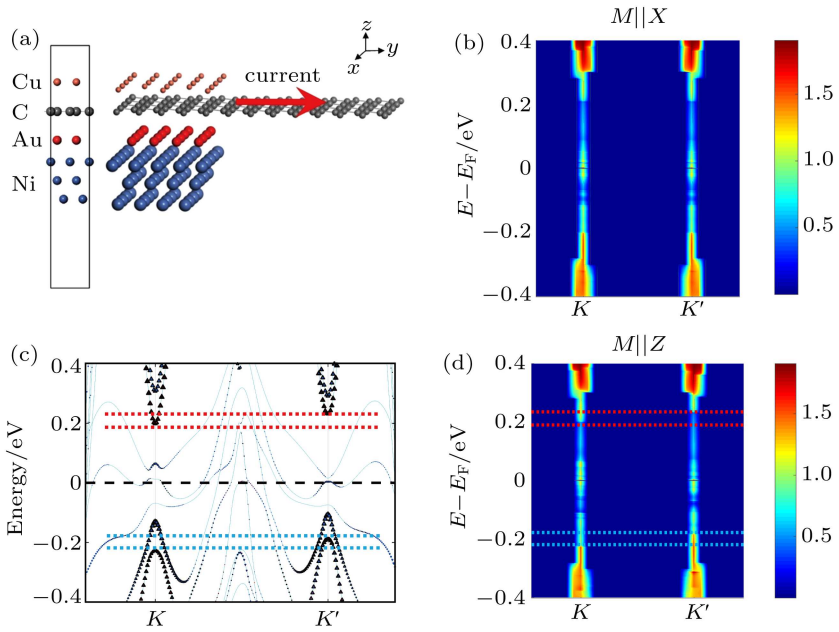


Fig. 3. Structure model of the transport system and the (E, k_x)-resolved transmission coefficients. (a) Model of the Cu/graphene/Au/Ni heterostructure. The current direction is presented by a red arrow. (b)(d) The (E, k_x)-resolved transmission coefficients for $M \parallel X$ and $M \parallel Z$, respectively. (c) Band structure of the left lead. The red and the blue dotted lines in (c) and (d) represent the regions where the valley splitting occurs.

In Figs. 4(a) and 4(b), we plot the valley-polarized current under finite bias, using the non-equilibrium formula

$$I_\tau = \frac{e}{h}\int_{-\infty}^{+\infty} T_\tau(E)\,[f_{\rm L}(E,\mu_{\rm L}) - f_{\rm R}(E,\mu_{\rm R})]\,{\rm d}E,$$

where I_τ is the valley-polarized current with $\tau = K$ or K', e is the electron charge, h is the Planck's constant, $T_\tau(E)$ denotes the transmission coefficients at the two valleys, and $f(E, \mu)$ is the Fermi–Dirac distribution at the energy of E with the chemical potential μ. The chemical potentials at the left lead ($\mu_{\rm L}$) and the right lead ($\mu_{\rm R}$) have the following relation with the bias voltage V: $\mu_{\rm L} - \mu_{\rm R} = eV$. Note that all the calculations are performed at the temperature of 0 K. As Fig. 4(a) shows, when $M \parallel X$, the I–V curves of the two valleys are completely identical, showing valley-degeneracy. However, when $M \parallel Z$ as shown in Fig. 4(b), the I–V curves at the K and K' points exhibit obvious difference, which means valley polarization. The inset of Fig. 4(b) shows the valley injecting efficiency, defined as $\eta = (I_K - I_{K'})/(I_K + I_{K'})$. When $M \parallel X$, η equals zero due to the degeneracy. But when $M \parallel Z$, we obtain distinct η values with the maximum of 10%.

Based on the unique property of this heterojunction/graphene contact system that the current is valley degenerate when $M \parallel X$ and valley polarized when $M \parallel Z$, we can imagine a valleytronic device. The left lead is a Cu/graphene/Au/Ni heterojunction to generate a valley-polarized current, which can be easily controlled by the magnetization direction of Ni. The right lead is a graphene to detect the valley-polarized current by the valley Hall effect that carriers at opposite valleys will acquire opposite anomalous velocities in the directions transverse to the electric field,[8] which has been realized in graphene and MoS_2 systems.[9,16] Thus, the valley-polarized current will induce the accumulation of different amounts of carriers with opposite valley polarizations at the opposite transverse edges of the graphene lead, then the finite valley Hall voltage appears, which can be easily detected by a voltmeter.

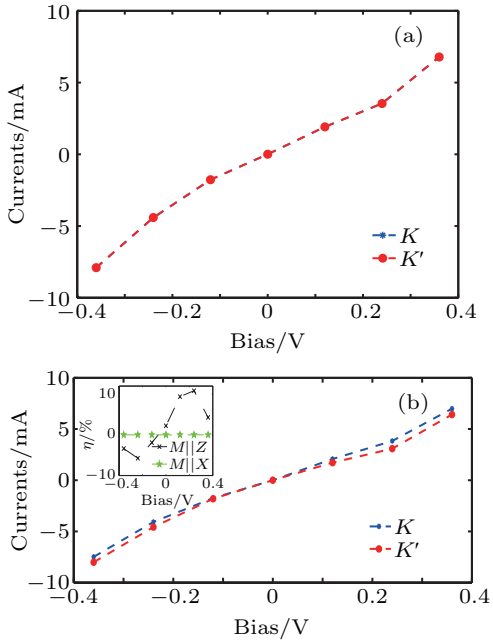


Fig. 4. Valley-polarized transport properties for the system shown in Fig. 3(a). (a), (b) The valley-dependent I–V characters when $M \parallel X$ and $M \parallel Z$, respectively. The inset in (b) shows the valley-injecting efficiency (η) when $M \parallel X$ and $M \parallel Z$.

4. Conclusion and perspectives

In the Ni/graphene heterostructure, the valley splitting is small and the π states of the graphene are destroyed because of the strong hybridization with the Ni, which is harmful for the use as a practical valley injector. By intercalating a monolayer Au, we can largely preserve the π states and enhance the valley splitting. However, the short-range graphene–Au interaction leads to charge transfer from the graphene to the Au, making a shift of the conical points with respect to the Fermi level.[28] To offset the shift, we use a Cu monolayer covering the graphene to compensate electrons. As a result, the Cu/graphene/Au/Ni heterojunction shows perfect valley injecting property.

From the viewpoint of practical application, our device has the following advantages. Firstly, the valley energy splitting is as large as 50 meV, which enables the device to work at room temperature. Next, the graphene π bands are largely preserved, which is very important because many peculiar properties of graphene are originated from the π states. Additionally, the valley-injecting states can be controlled simply by changing the magnetization direction of Ni, and detected easily by the valley Hall effect. Because of the large separation comparable to the size of the BZ in the momentum space,[29–31] the inter-valley scattering is strongly suppressed and the valley-injecting length is long, which means experimental realization is much possible. This valley injection concept and method could be extended to other 2D materials and might open an opportunity of room-temperature valleytronics.

References

[1] Novoselov K S, Geim A K, Morozov S V, Jiang D, Zhang Y, Dubonos S V, Grigorieva I V and Firsov A A 2004 *Science* **306** 666
[2] Geim K and Novoselov K S 2007 *Nat. Mater.* **6** 183
[3] Rycerz, Tworzydlo J and Beenakker C W J 2007 *Nat. Phys.* **3** 172
[4] Gunlycke D and White C T 2011 *Phys. Rev. Lett.* **106** 136806
[5] Jiang Y, Low T, Chang K, Katsnelson M I and Guinea F 2013 *Phys. Rev. Lett.* **110** 046601
[6] Hu C, Lu W, Ji W, Yu G, Yan Y and Teng J 2015 *Phys. Rev. B* **92** 115404
[7] Xiao D, Yao W and Niu Q 2007 *Phys. Rev. Lett.* **99** 236809
[8] Shimazaki Y, Yamamoto M, Borzenets I V, Watanabe K, Taniguchi T and Tarucha S 2015 *Nat. Phys.* **11** 1032
[9] Aivazian G, Gong Z, Jones A M, Chu R L, Yan J, Mandrus D G, Zhang C, Cobden D, Yao W and Xu X 2015 *Nat. Phys.* **11** 148
[10] Srivastava A, Sidler M, Allain A V, Lembke D S, Kis A and Imamoğlu A 2015 *Nat. Phys.* **11** 141
[11] Cai T, Yang S A, Li X, Zhang F, Shi J, Yao W and Niu Q 2013 *Phys. Rev. B.* **88** 115140
[12] MacNeill D, Heikes C, Mak K F, Anderson Z, Kormányos A, Zólyomi V, Park J and Ralph D C 2015 *Phys. Rev. Lett.* **114** 037401
[13] Mak K F, He K, Shan J and Heinz T F 2012 *Nat. Nanotechnol.* **7** 494
[14] Mak K F, McGill K L, Park J and McEuen P L 2014 *Science* **344** 1489
[15] Suzuki R, Sakano M, Zhang Y J, Akashi R, Morikawa D, Harasawa A, Yaji K, Kuroda K, Miyamoto K, Okuda T, Ishizaka K, Arita R and Iwasa Y 2014 *Nat. Nanotechnol.* **9** 611
[16] Wu S, Ross J S, Liu G B, Aivazian G, Jones A, Fei Z, Zhu W, Xiao D, Yao W, Cobden D and Xu X 2013 *Nat. Phys.* **9** 149
[17] Jones A M, Yu H, Ghimire N J, Wu S, Aivazian G, Ross J S, Zhao B, Yan J, Mandrus D G, Xiao D, Yao W and Xu X 2013 *Nat. Nanotechnol.* **8** 634
[18] Zeng H, Dai J, Yao W, Xiao D and Cui X 2012 *Nat. Nanotechnol.* **7** 490
[19] Xu X, Yao W, Xiao D and Heinz T F 2014 *Nat. Phys.* **10** 343
[20] Kang M H, Jung S C and Park J W 2010 *Phys. Rev. B.* **82** 085409
[21] Taylor J, Guo H and Wang J 2001 *Phys. Rev. B* **63** 245407
[22] Maassen J, Ji W and Guo H 2010 *Appl. Phys. Lett.* **97** 142105
[23] Perdew J P and Zunger A 1981 *Phys. Rev. B.* **23** 5048
[24] Varykhalov A, Sánchez-Barriga J, Shikin A M, Biswas C, Vescovo E, Rybkin A, Marchenko D and Rader O 2008 *Phys. Rev. Lett.* **101** 157601
[25] Varykhalov A, Scholz M R, Kim T K and Rader O 2010 *Phys. Rev. B.* **82** 121101
[26] Marchenko D, Varykhalov A, Scholz M R, Bihlmayer G, Rashba E I, Rybkin A, Shikin A M and Rader O 2012 *Nat. Commun.* **3** 1232
[27] Giovannetti G, Khomyakov P A, Brocks G, Karpan V M, J van den Brink and Kelly P J 2008 *Phys. Rev. Lett.* **101** 026803
[28] Khomyakov P A, Giovannetti G, Rusu P C, Brocks G, J van den Brink and Kelly P J 2009 *Phys. Rev. B.* **79** 195425
[29] Morozov S V, Novoselov K S, Katsnelson M I, Schedin F, Ponomarenko L A, Jiang D and Geim A K 2006 *Phys. Rev. Lett.* **97** 016801
[30] Gorbachev R V, Tikhonenko F V, Mayorov A S, Horsell D W and Savchenko A K 2007 *Phys. Rev. Lett.* **98** 176805
[31] Xiao D, Liu G B, Feng W, Xu X and Yao W 2012 *Phys. Rev. Lett.* **108** 196802